Thermal, structural and optical properties of {CdS}–$Na_{86}X$ composites

Gerardo Gutiérrez-Juárez,[a] Orlando Zelaya-Angel,[a] Juan J. Alvarado-Gil,[a] Helion Vargas,[a]* Heloise de O. Pastore,[b] José S. Barone,[b] Manuel Hernandez-Velez[c] and Leticia Baños[d]

[a] *Departamento de Física, CINVESTAV-IPN, A. P. 14-740 México D. F. 07000, México*
[b] *Instituto de Química, Universidade Estadual de Campinas, CP 6154, CEP 13083-970, Campinas, S. P., Brazil*
[c] *Instituto Superior Pedagógico E. J. Varona, La Habana, Cuba*
[d] *IIM-UNAM, C. P. 703, México D. F. 04511, México*

Thermal, structural and optical properties of CdS superclusters grown in zeolite $Na_{86}X$ are reported. The interest in this work arose in the need to study CdS prepared in the zeolite host, at high concentrations (>19%), in order to observe porosyte behaviour and CdS aggregate properties. The semiconductor–zeolite composite was studied using X-ray diffraction analysis and photoacoustic technique (PAS). The properties of semiconductor CdS embedded in a zeolite matrix were analysed as a function of the CdS concentration by monitoring Cd concentration (atom%) by chemical analysis. The results show that as the concentration of CdS increases, the thermal diffusivity, capacity, conductivity and the band-gap increase up to a point where the zeolite lattice collapses. From this point on, all these thermal properties diminish and the band-gap is the same as for bulk CdS.

In recent years, many efforts have been made to study the physical properties of semiconductor clusters, and in particular CdS, embedded in zeolite matrices. The main trends in these works have been to investigate the optical and structural properties of the semiconductor encapsulated in the zeolites, and how they are influenced by quantum size effects.[1–4]

Zeolites are crystalline aluminosilicates that have a regular pore and/or channel structure of the order of atomic dimensions.[5] Introducing aluminium atoms into silica networks yields a negative charge. The charge-balancing cations are loosely bound to framework oxygen atoms and can be readily exchanged in most cases for other cations. Water molecules are also present in the cavities of zeolites and can freely move, favouring ion exchange and reversible dehydration.[6] Zeolites with the appropriate combination of molecularly sized holes and cation exchange ability have found a great number of uses in the chemical industry.[7–9] In the electronic industry, semiconductor clusters encapsulated in zeolites have significant potential applications *e.g.* in solar energy conversion, photocatalysis and in high density information storage.[10–13]

Thermal diffusivity and optical absorption coefficients are unique to each material as can be appreciated from tabulated values of α provided by Touloukian *et al.*[14] for a wide range of materials (metals, minerals, semiconductors, biological specimens, *etc*). Furthermore, thermal diffusivity is also known to be extremely dependent upon the effects of compositional variables,[15] as well on the processing conditions used to prepare polymers,[16,17] ceramics[15] and glasses.[18]

The photoacoustic (PA) effect[19,20] has proved[21–23] to be a reliable technique for measuring thermal diffusivity and absorption spectra of solid samples although at present there seems to be no data relating the thermal properties of semiconductors in zeolites.

In this paper we report thermal properties and optical spectra of CdS prepared in zeolite $Na_{86}X$ at high concentrations (>19%). Our measurements have been complemented by X-ray diffraction and chemical analysis.

Experimental

Sample preparation

The zeolite used in these work was a commercial synthetic material from Laporte with a silicon: aluminum ratio of 1.23 : 1 and of formula $Na_{86}Al_{86}Si_{106}O_{384}\cdot 250H_2O$. The relative concentration of CdS inside the zeolite host ranged from the supercluster limit[4] to a mixture of the zeolite with the semiconductor. {CdS}–$Na_{86}X$ powder composites were prepared by chemical synthesis and their crystalline structure was established by X-ray diffraction analysis.

Syntheses of samples of {CdS}–$Na_{86}X$ were carried out as follows: 2η g of zeolite powder were added to 0.1 mol dm^{-3} ammonium nitrate solution and stirred well at 363 K, during 5 h, in order to effect ion exchange. Then the solution was filtered and extensively washed with deionized water. The solid obtained was mixed with water and to this suspension, 2η g of thiourea and η g of cadmium chloride were added and vigorously stirred during 2 h, at 363 K. The solid was then filtered, thoroughly washed with deionized water and air-dried. The CdS concentration in the composite is a function of the parameter η.

X-Ray analysis

The crystalline structure of the samples was established by X-ray diffraction using a Siemens D-500 diffractometer monitored at 35 kV and 15 mA, with Cu-Kα radiation ($\lambda = 0.15406$ nm) at a scan speed of 1 degrees min^{-1} (in 2θ) with Diffrac-AT software [version 3.2, SOCABIM (1993)] with a sample surface area of 6.45 cm^2; JCPDS PDF 41-1049 for CdS was used to reference the peaks.

PA technique

The PA effect looks directly at heat generated in a sample due to non-radiative deexcitation processes following the absorp-

tion of light. In a conventional experimental arrangement, a sample is enclosed in an air-tight cell and exposed to a chopped light beam. As a result of the periodic heating of the sample, the pressure in the cell oscillates at the chopping frequency and can be detected by a sensitive microphone coupled to the cell. The resulting signal depends not only on the amount of heat generated in the sample (and, hence, on the optical absorption coefficient and the light-into-heat conversion efficiency of the sample) but also on how the heat diffuses through the sample, as determined by the thermal diffusivity.

Optical spectra

The photoacoustic absorption spectra were obtained in the region 350–750 nm by the use of a standard photoacoustic spectrometer. The experimental set-up used consists of a 1000 W xenon lamp (Oriel), a variable-frequency chopper set at 17 Hz, a monocromator, an air-filled aluminium cell with a condenser microphone, a low-noise preamplifier, and a lock-in amplifier. The sample compartment, in which the powdered {CdS}–$Na_{86}X$ composite was placed, is a cylindrical chamber. The photoacoustic signal is preamplified before providing the input to the signal channel lock-in amplifier (SR-850). The resultant photoacoustic spectra are recorded in a computer, which simultaneously displays the wavelength-dependent signal intensity.

Thermal diffusivity, α

The thermal diffusivity, α, is the quantity that measures the rate of diffusion of heat in a material. Apart from its own intrinsic importance, its determination provides the value of the thermal conductivity, k, if the density, ρ, and the heat capacity at constant pressure, C_p, are known ($\alpha = k/\rho C_p$). Physically, the inverse of α is a measure of the time required to achieve thermal equilibrium in a given material.

In order to perform the photoacoustic measurements for thermal diffusivity, circular pieces of the composite powder (300 μm thick, 3 mm radius) were prepared by pressing the powder at a pressure of 5.1×10^3 atm.

The experimental arrangement for the PA measurements of the thermal diffusivity is shown schematically in Fig. 1. It consists of an Oriel 250W halogen lamp the polychromatic beam of which is mechanically chopped and focused onto the sample. The sample is mounted in such a way as to cover the opening of the microphone as shown in Fig. 1. The signal from the microphone is connected to a lock-in amplifier used to register both the signal amplitude and the phase; these were recorded as a function of the modulation frequency. The above arrangement corresponds to a heat transmission configuration. That is, the deposited heat at the rear-side face of the sample diffuses through the sample before reaching the PA chamber where it causes pressure fluctuations that are detected by the microphone. All measurements were performed putting a thin circular Al foil (3 mm diameter, 15 μm

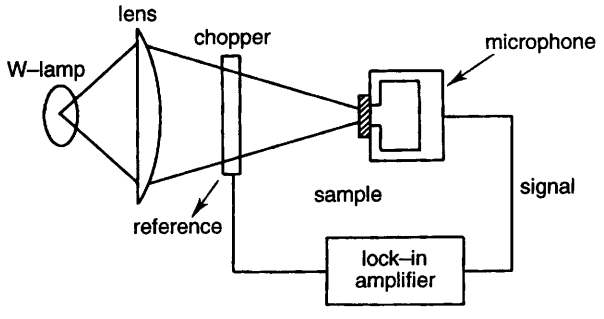

Fig. 1 Schematic arrangement for the PA measurements of thermal diffusivity

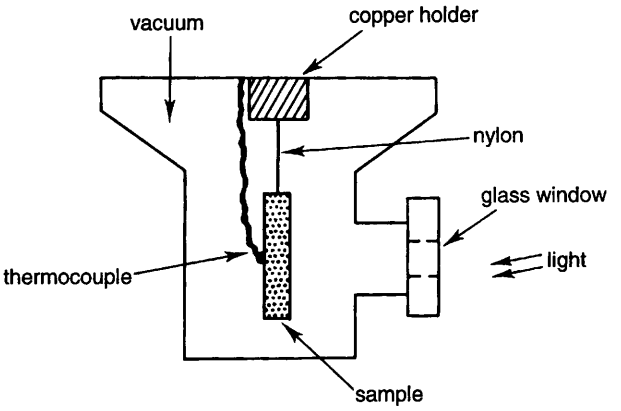

Fig. 2 Experimental arrangement for measuring the heat capacity per volume unit using the temperature-rise method under continuous light illumination

width) attached with thermal paste on the light incident side, in order to guarantee opaque conditions implicit in the theory.[24] The thermal diffusion time $\pi l^2/\alpha_{Al}$ in the Al foil is of the order of *ca.* 7 μs ($\alpha_{Al} = 0.92$ cm^2 s^{-1}), so that the heat absorbed in the Al foil may be assumed to be instantaneously transmitted to the sample. The thermal wave attenuation in the sample is essentially determined by the sample thermal diffusivity α.

Heat capacity, ρC_p

The heat capacity per unit volume, ρC_p, was measured using the temperature rise method, under continuous white-light illumination. The experimental arrangement is shown in Fig. 2. The samples were sprayed on both surfaces with a very thin film of black paint. A light-absorbing surface and the same heat-transfer coefficient were thus assured for each side of the sample. The samples were adiabatically suspended in a Dewar flask which was subsequently vacuum sealed. Under these conditions, the main heat-loss mechanism was by radiation. The Dewar had an entrance glass window through which the continuous white-light beam was focused onto one of the sample surfaces. A thermocouple was attached on the opposite surface using thermal paste. In this way, the temperature evolution of the back surface could be monitored as a function of the time. Care has been taken to prevent the heating light from reaching the thermocouple. Since the samples thicknesses are typically in the order of 300 μm and much smaller than their widths (*e.g.* 0.6 cm), the simple one-dimensional heat diffusion equation with radiation losses could be applied to our measurements. Solving the one-dimensional heat diffusion equation,[25] it can be shown that the long-term time evolution (*i.e.*, for times greater than the heat diffusion time, approximately l^2/α, where l is the sample thickness and α the thermal diffusivity) of the back surface temperature rise is given by:

$$\Delta T = (I_0 \alpha\tau/lk)[1 - \exp(-t/\tau)] \quad (1)$$

where I_0 is the intensity of the incident light beam and $\tau = l\rho C_p/2H$ is the rise time. Here, $H = 4\sigma T_0^3$, where σ is the Stefan–Boltzmann constant, T_0 is the ambient temperature, and H is the radiation heat transfer coefficient. τ is determined by fitting the experiental result with eqn. (1). The thermal conductivity k is readily obtained from the previously value of α calculated by using $k = \alpha\rho C_p$.

Results and Discussion

Chemical and X-ray diffraction analysis

The parameter η was fixed to values of 0.05, 0.10, 0.20, 0.50 and 0.80. Fig. 3(*a*) and (*b*) illustrate the plot of number of Cd

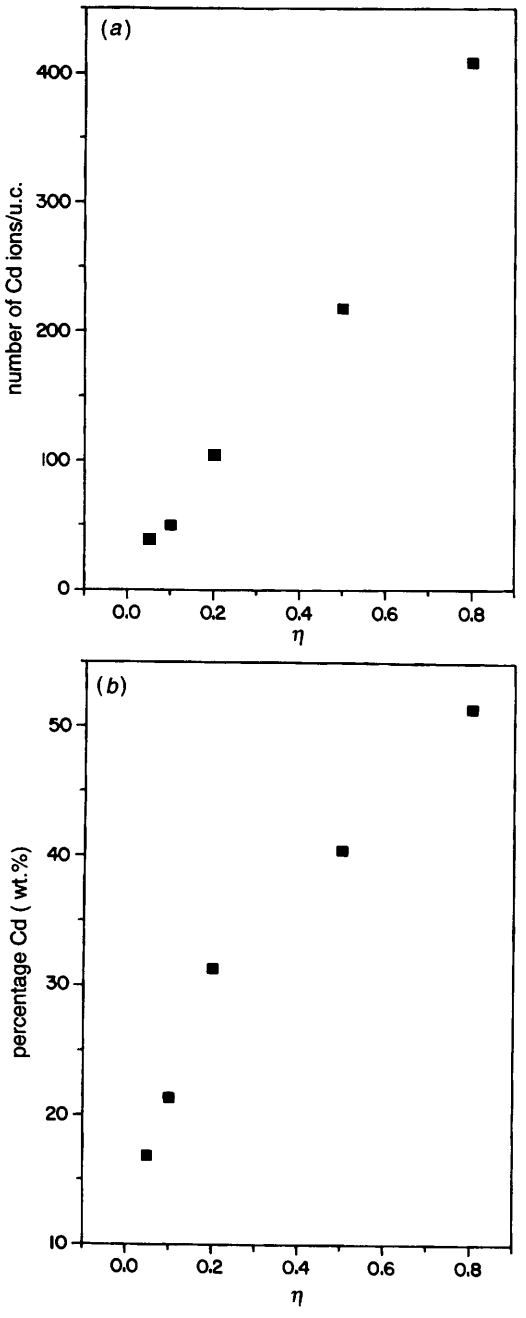

Fig. 3 Measurements by chemical analysis. (*a*) Plot of number of Cd ions per unit cell and (*b*) wt.% of CdS.

ions per unit cell and wt.% CdS, measured by chemical analysis, as a function of η. Table 1 lists the different obtained Cd percentages for each η. From these data, it can be observed that the concentration of CdS for the first sample is at the limit of the unit-cell capacity of ion exchange, taking into account all its cationic sites. In the other samples, the CdS concentration is well over this limit, leading to the conclusion that CdS crystallites are forming into and around the zeolite crystals and at these CdS concentrations superclusters are formed.

Table 1 The η parameter, percentage of Cd, lattice parameter and E_g values for {CdS}–$Na_{86}X$ zeolites

η	Cd (%)	a_0/Å	E_g/eV
0.05	16.96	24.9 ± 0.1	2.36 ± 0.03
0.10	21.40	24.8 ± 0.1	2.43 ± 0.03
0.20	31.40	25.0 ± 0.3	2.46 ± 0.03
0.50	40.56	amorphous	2.34 ± 0.03
0.80	51.51	amorphous	2.34 ± 0.03

Superclusters are viewed as three-dimensional arrays of mutually interacting clusters (quantum dots) with their geometric structure imposed by the zeolite internal pore structure.[3] From IR spectroscopy measurements, it has been found that CdS superclusters have to be strongly coupled to the zeolite lattice.[4] This strong coupling arises from the interactions among clusters through the zeolite framework. In our samples, all measurements were performed after the CdS cluster interaction has overcome the critical threshold at which, statistically, these clusters must now populate adjacent cluster positions, giving origin to the superclusters. The critical threshold appears at 4 ± 1 wt.%, inside the sodalite cages of the Y zeolite;[2] the cages in X and Y zeolites are about the same size.[26] An observed abrupt transition in optical absorption measurements suggests that the cluster aggregation process may be a three-dimensional percolation process.[2] Based on the this consideration, it is expected in our case that increasing the CdS concentration leads to the entire zeolite structure suffering an increasing internal pressure. This effect is due to the growth of population in neighbouring cluster positions and their interactions throughout the zeolite lattice. If the interactions among clusters continues to grow, there will be a point where the zeolite framework cannot withstand the internal pressure and result in crumbling. This was confirmed by powder X-ray diffraction.

Fig. 4 shows the X-ray profiles of samples from 16.96 to 40.56 wt.%. The pattern of pure $Na_{86}X$ and hexagonal CdS are included for comparison. Fig. 4(*a*) shows the zeolite diffraction diagram, the crystalline lattice of which has cubic symmetry. Fig. 4(*b*)–(*e*) display the patterns of composites with increasing CdS concentration. It can be observed that even at only 16.96 wt.% CdS, peaks belonging to the semiconductor crystalline phase are superimposed with peaks corresponding to the zeolite. Upon increasing the CdS concentration, X-ray analysis shows that peaks corresponding to the zeolite phase become less intense, and those identified with CdS are better defined. In Fig. 4(*e*), only the CdS contribution appears in the range of 2θ where the zeolite usually presents a crytalline pattern and no clear features are observed for the zeolite. Therefore, we conclude that the zeolite becomes amorphous. The same behaviour was observed for the sample with 51.51 wt.% Cd.

As expected, the evaluation of the zeolite lattice parameter a is encumbered by the significant presence of CdS clusters. Table 1 lists values of a, together with the standard deviations; all the values are the same within statistical deviation.

Determination by the photoacoustic technique of band-gap energy value (E_g)

The photoacoustic absorption spectra of four samples are shown in Fig. 5. For the band-gap energy value (E_g) determination we chose the 'knee' criterion.[27] Theoretical models for a more exact calculation of E_g from photoacoustic data are reported in the literature,[28] however, we are only interested in the general trends of E_g in the composites studied. The use of the 'knee' method is illustrated in the insert of Fig. 5 and E_g values for the samples are listed in Table 1. Fig. 6 illustrates the E_g values as a function of the wt.% CdS. The $Na_{86}X$ zeolite is an insulator, thus its E_g value is expected to be larger than 3.54 eV, the limit of detection of our experimental set-up. The E_g value for pure powdered CdS was measured by this technique and found to be 2.36 ± 0.03 eV. E_g values for 16.96, 40.56 and 51.51 wt.% {CdS}–$Na_{86}X$ composites are nearly the same as for pure CdS. That means that at these concentrations there are no quantum size effects. However, at 21.40 and 31.40 wt.%, just prior to the total colapse of the zeolite structure, E_g is higher than that of pure CdS indicating that at

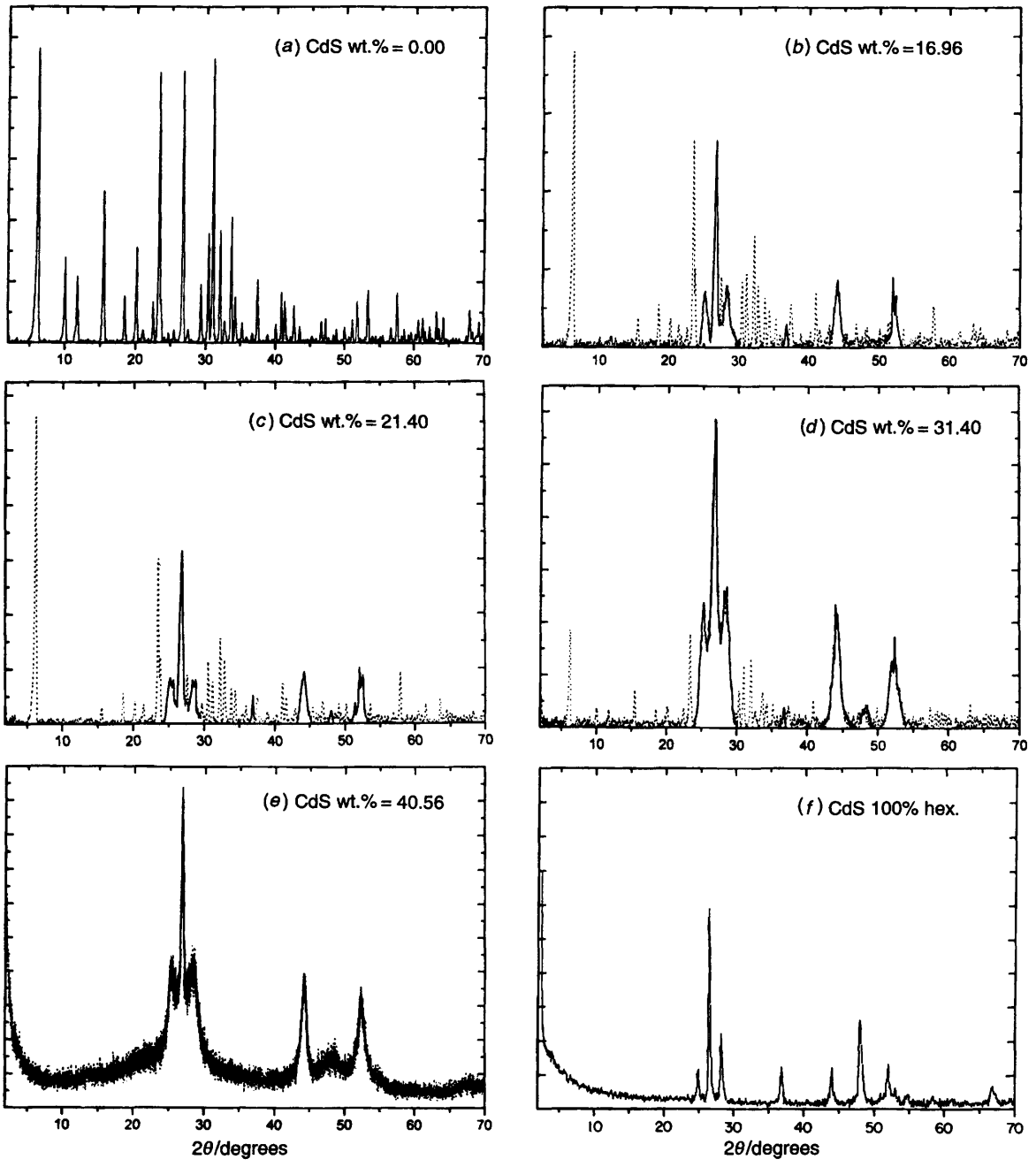

Fig. 4 X-Ray diffractograms. (*a*) Pure zeolite, (*b*)–(*e*) Samples with 10.96, 21.40, 31.40 and 40.56 wt.% CdS respectively, in these four diffractograms the solid lines are the peaks of the CdS phase and the dashed lines arise from the crystalline structure of the zeolite; (*f*) pure hexagonal CdS.

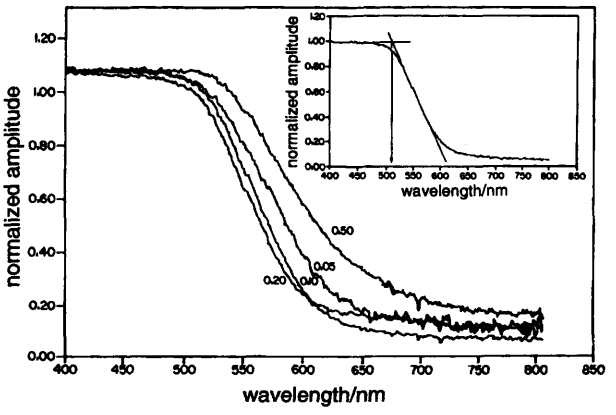

Fig. 5 Photoacoustic absorption spectra for $\eta = 0.05$, 0.10, 0.20 and 0.50

these concentrations, although the clusters are not small, there is a quantum size-type influence on E_g values. This dependence can be explained by considering that at these concentrations, the CdS clusters in the zeolite are under pressure and are strongly interacting with each other. Therefore, it is expected that the CdS clusters experiment a shrinkage. An immediate consequence of this is to obtain E_g values. After amorphitization of the zeolite, for the 40.56 and 51.51 wt.% composites, the composites are a mixture of silicoaluminate with crystalline aggregates of CdS and E_g values measured for these mixtures, obviously, must be closer to that corresponding to crystalline CdS. For CdS concentrations in the range 16.96–31.40, we are confident that the CdS has not lost its chemical identity inside the cages. In other words, the formation of a new chemical compound from zeolite and CdS can be ruled out, since X-ray analysis does not show any pattern corresponding to a different crystalline substance. The same analysis is valid for CdS concentrations higher than 31.40

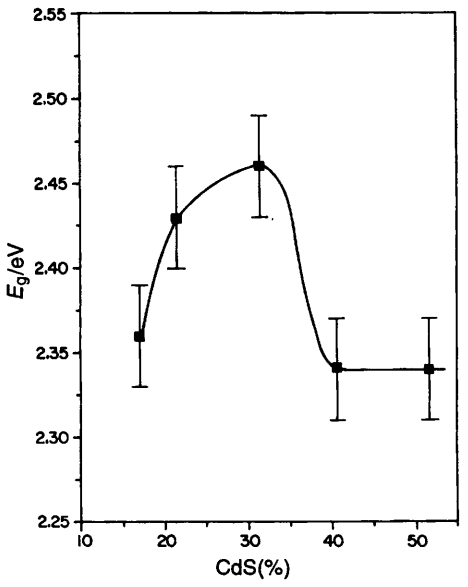

Fig. 6 Energy band-gap values of the samples as a function of % CdS

wt.%. Hence it can be concluded that we are essentially measuring E_g for the CdS encapsulated in $Na_{86}X$ zeolite up to a limiting content of 31.40%.

Measurement of thermal properties

In the thermal diffusivity (α) measurements using the OPC detector, the pressure fluctuation δp in the air chamber, for the rear-side illumination configuration, Fig. 1, is predicted by the thermal diffusion model[24] and given by

$$\delta p \approx \frac{\gamma P_0 I_0 (\alpha_g \alpha_s)^{1/2}}{2\pi l_g T_0 k_s f} \left\{ \frac{\exp[j(\omega t - \pi/2)]}{\sin h(l_s \sigma_s)} \right\} \quad (2)$$

where γ is the air heat capacity ratio, $P_0(T_0)$ is the ambient pressure (temperature), I_0 is the radiation intensity, f is the modulation frequency and l_i, k_i and α_i are the length, thermal conductivity and thermal diffusivity of medium i, respectively. Here, the subscript i denotes the absorbing sample (s) and the air (g), respectively. $\sigma_i = (1 + j)a_i$, $a_i = (\pi f/\alpha_i)^{1/2}$ is the complex thermal diffusion coefficient of material i. In arriving at eqn. (2) we have assumed that the sample is optically opaque to the incident radiation and that the heat flux into the surrounding air is negligible. The optical opaqueness condition means that all the radiation is absorbed at the outer sample surface ($z = -l/2$ in Fig. 7). Eqn. (2) is further simplified in two limiting cases depending upon the thermal properties of the sample. For a thermally thin sample, namely $l_s a_s \ll 1$, it reduces to:

$$\delta p \cong \frac{\gamma P_0 I_0 (\alpha_g^{1/2} \alpha_s)}{2\pi l_g T_0 k_s l_s} \left\{ \frac{\exp[j(\omega t - 3\pi/4)]}{f^{3/2}} \right\} \quad (3)$$

i.e. the detected signal should decrease as $f^{3/2}$ as one increases

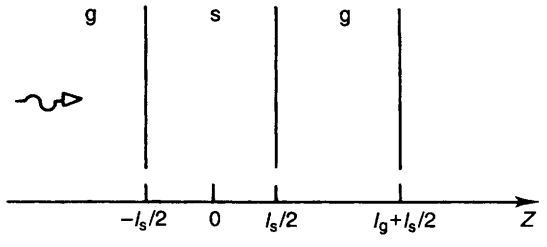

Fig. 7 Schematic geometry for the PA signal generation in which the incident light beam of intensity I_0 is fully absorbed at $z = -l_s/2$

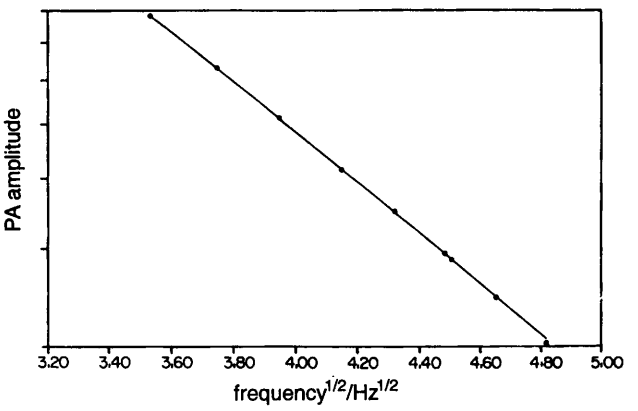

Fig. 8 OPC signal amplitude, as a function of the modulate square root of the frequency. The solid line represents the best fit of the data to eqn. (5).

the modulation frequency. If $l_s a_s \gg 1$, the samples are thermally thick, and one obtains:

$$\delta p \cong \frac{\gamma P_0 I_0 (\alpha_g \alpha_s)^{1/2}}{\pi l_g T_0 k_s} \left\{ \frac{\exp[-l_s(\pi f/\alpha_s)^{1/2}]}{f} \right\} \times \exp[j(\omega t - \pi/2 - l_s a_s)] \quad (4)$$

Eqn. (3) means that, for a thermally thick sample, the amplitude of the PA signal decreases exponentially with the modulation frequency as $(1/f)\exp(-af^{1/2})$, where $a = (\pi l_s^2/\alpha_s)^{1/2}$. From eqn. (3) and (4) the thermal diffusivity α_s can be obtained by fitting the data in the corresponding regime. However, in the thermally thick regime, small changes in the diffusivity give place to larger changes in the PA signal. In this regime α_s can be obtained by fitting the experimental data with the coefficient b, by using eqn. (4) in the form:

$$S = \left(\frac{A}{f}\right)\exp(-bf^{1/2}) \quad (5)$$

The constant A, in the measured signal S, apart from geometric factors, includes all other factors such as the gas thermal properties, and so on. We thus have two adjustable parameters A and b to describe the PA monitoring of the thermal diffusivity of the sample.

In Fig. 8, we show the PA signal amplitude as a function of the modulated square root of the frequency for 51.51 wt.% CdS sample. The solid curve in this Figure represents the fitting of the experimental data to eqn. (5). The resulting value of α from the data fitting was $(2.60 \pm 0.31) \times 10^{-3}$ cm^2 s^{-1}. Table 2 lists the α results from 0 to 51.51 wt.% CdS. The α *vs.* CdS wt.% results are plotted in Fig. 9(*a*); as can be observed, three regions can be observed: the unloaded, uncollapsed sample (0 wt.% CdS); the loaded, uncollapsed samples (16.96–31.40 wt.%) and the heavily loaded, totally amorphous samples (40.56 and 51.51 wt.%). The behaviour of α as a function of CdS wt.% can be explained by considering that from 0 to 24 CdS wt.%, the density of the material is increasing, *i.e.*

Table 2 Thermal parameters as functions of percentage of CdS

CdS (wt.%)	α /10^{-3} cm^2 s^{-1}	ρC_p /W s cm^{-3} K^{-1}	k /10^{-3} W cm^{-1} K^{-1}
0	1.40 ± 0.17	1.26 ± 0.15	1.76 ± 0.42
16.96	3.00 ± 0.14	1.16 ± 0.14	3.48 ± 0.84
21.40	2.60 ± 0.31	1.27 ± 0.15	3.30 ± 0.79
31.40	3.40 ± 0.41	2.68 ± 0.32	9.11 ± 2.20
40.56	2.10 ± 0.25	1.45 ± 0.17	3.05 ± 0.73
51.51	1.50 ± 0.18	1.80 ± 0.21	2.70 ± 0.65

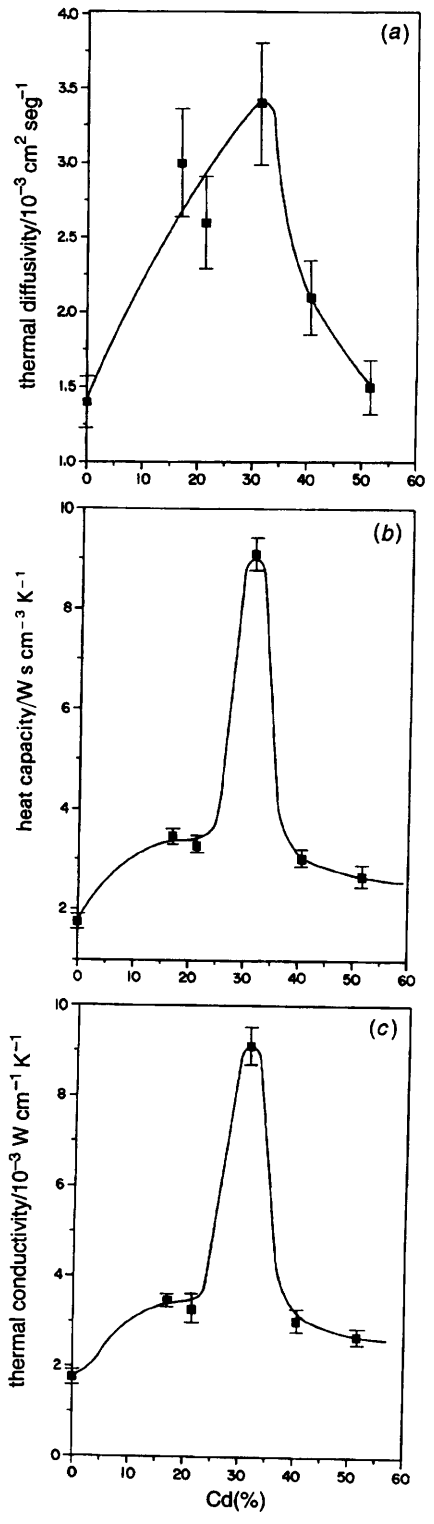

Fig. 9 (*a*) Thermal diffusivity, (*b*) heat capacity and (*c*) thermal conductivity *a* as a function of CdS content

the zeolite becomes less porous as CdS wt.% increases. The minimum crystallinity of the composite is conserved in that range. Under these conditions, it is expected that heat flowing is faster. Thus the diffusivity α increases as CdS wt.% increases as has been reported for ceramic materials.[29] For CdS wt.% > 31.40, the zeolite becomes amorphous, and heat does not flow as easily as for the samples with CdS wt.% < 31.40. The loss of crystallinity in the composite is an impediment for effective heat transfer, despite the probable higher density. Fig. 9(*a*) clearly shows that α diminishes for CdS wt.% > 31.40.

Fig. 10 shows the back surface temperature rise as a function of time, after commencement of illumination, for a sample with wt.% CdS = 21.40. This Figure also shows the cooling of the back surface of the sample when the illumination is switched off. The solid line in Fig. 10 represents the result of the best fit of the experiental data to eqn. (1) using τ as an adjustable parameter. From the value of τ obtained in this way, one obtains the experimental value of the heat capacity from ρC_p, for the sample with 21.40 wt.% CdS. The same procedure was followed in order to obtain the ρC_p values for all the sample. ρC_p values are given in Table 2 and ρC_p *vs.* wt.% CdS is plotted in Fig. 9(*b*). It is known that both crystalline and amorphous phases of the same compound have nearly equal heat capacities.[30] However, in the vicinity of a phase transition, the behaviour is different. As can be observed in Fig. 9(*b*), the heat capacity of wt.% 31.40 sample abruptly separates from the remainder of the ρC_p value. We know that this concentration is at a critical limit for the zeolite integrity, above which the crystalline-to-amorphous phase transition occurs. This is consistent with the well known behaviour of heat capacity at critical points. This is an obvious example of detection of a phase transition from measurements of heat capacity per unit volume.

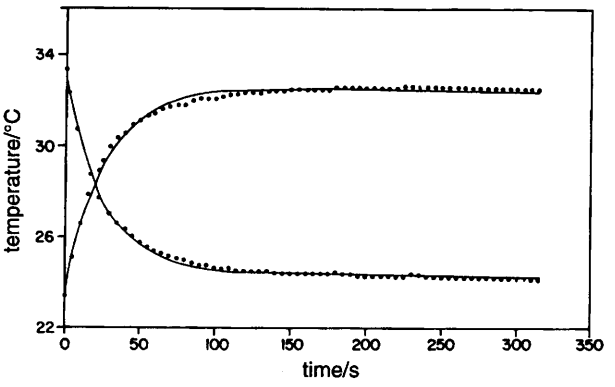

Fig. 10 Back surface temperature evolution for a sample with CdS wt.% = 21.40. The solid line represents the result of the best fit of the experimental data to eqn. (1) using τ as an adjustable parameter.

Fig. 9(*c*) shows the thermal conductivity *k* as a function of percentage CdS and Table 2 lists the *k* values for all the CdS percentages used. It is evident from Fig. 9(*c*) and Table 2 that *k* reaches a maximum at 31.40 wt.%. The analysis of this phenomenon is essentially the same as for the values of α. Heat flows faster through a less porous crystalline material than in a more porous or amorphous material. Hence, a larger amount of heat flows per unit time for the 31.40 wt.% CdS composite.

Conclusion

In summary, we have investigated the CdS superclusters encapsulated in $Na_{86}X$ matrices, from lower concentrations to higher concentrations which make the zeolite amorphous. This phase transition has been attributed to the interaction between clusters throughout the zeolite framework. Even though the arrangements of the CdS clusters is not yet clearly understood, increase in the CdS concentration causes a build up of stresses to a critical point beyond which the crystalline structure collapses; CdS crystallinity is conserved for all concentrations used. Photothermal techniques allowed us to obtain the energy band-gaps, E_g, of the samples and their thermal properties: diffusivity, α, heat capacity, C_p and conductivity, *k*, as a function of the CdS concentration (embedded in the zeolite framework). All the curves obtained (for E_g, α, *k* and ρC_p) showed a maximum for a critical concentration of 31.4 wt.% of CdS. The E_g behaviour is explained by considering that increasing the semiconductor concentration causes

also an increase in the interaction between CdS clusters (which gives origin to the superclusters). With corresponding lattice shrinkage, a rise in E_g is observed until a maximum is reached. Beyond this point, the structure of the zeolite becomes amorphous and E_g is that of bulk CdS. The maximum in the thermal parameters α and k is due to increasing CdS concentration, while decreasing porosity eases the heat flux through the material. In this way, α and k increase as the concentration increases, while the zeolite framework is preserved. It is evident that when the zeolite becomes amorphous the heat flow diminishes. The maximum in the heat capacity C_p is evidence of the crystalline-to-amorphous phase transition of the zeolite.

This work was partially supported by CONACyT-México. The authors are grateful to Ing. M. J. Guerrero, A. Buendia and A. Castillo for their technical assistance.

References

1 K. Moller, M. M. Eddy, G. D. Stucky, N. Herron and T. Bein, *J. Am. Chem. Soc.*, 1989, **111**, 2564.
2 N. Herron, Y. Wang, M. M. Eddy, G. D. Stucky, D. E. Cox, K. Moller and T. Bein, *J. Am. Chem. Soc.*, 1989, **111**, 530.
3 Y. Wang, N. Herron, W. Mahler and A. Suna, *J. Opt. Soc. Am. B*, 1989, **6**, 808.
4 Y. Wang and N. Herron, *J. Phys. Chem.*, 1988, **92**, 4988.
5 D. W. Breck, in *Zeolite Molecular Sieves*, 1974, Wiley, New York.
6 J. V. Smith, in *Zeolites Chemistry and Catalysis. ACS Monogr. 171*, ed. J. A. Rabo, 1976, ch. 1, II Series American Chemical Society.
7 R. Szostak, in *Molecular Sieves, Principles of Synthesis and Identification*, Van Nostrand Reinhold, New York, 1989; M. E. Davis and R. F. Lobo, *Chem. Mater.*, 1992, **4**, 975.
8 Z. Li, C. M. Wang, L. Persaud and T. E. Mellouk, *J. Phys. Chem.*, 1988, **92**, 2592.
9 Z. Li, C. Lai and T. E. Mallouk, *Inorg. Chem.*, 1989, **28**, 2592.
10 A. J. Bard, *J. Phys. Chem.*, 1982, **82**, 172.
11 M. Gratzel, *J. Chem. Soc., Faraday Trans. 1*, 1984, **80**, 183.
12 J. R. Darwent, *J. Chem. Soc., Faraday Trans. 1*, 1984, **80**, 322.
13 G. A. Ozin, A. Stein and G. D. Stucky, *J. Photograph. Sci. Jpn.*, 1990, **53**, 322.
14 Y. S. Touloukian, R. W. Powell, C. Y. Ho and M. C. Nicolassu, in *Thermal Diffusivity*, 1973, IFI/Plenum, New York.
15 G. Ziegler and D. P. Hasselman, *J. Mater. Sci.*, 1981, **16**, 495.
16 N. F. Leite, N. Cella, H. Vargas and L. C. M. Miranda, *J. Appl. Phys.*, 1987, **61**, 3023.
17 A. Torres-Filho, N. F. Leite, L. C. M. Miranda, N. Cella and H. Vargas, *J. Appl. Phys.*, 1989, **66**, 97.
18 A. C. Bento, H. Vargas and L. C. M. Miranda, *Phys. Chem. Glasses*, 1987, **61**, 127.
19 A. Rosencwaig, in *Photoacoustic and Photoacoustic Spectroscopy*, Wiley, New York, 1980.
20 H. Vargas and L. C. M. Miranda, *Phys. Rep.*, 1988, **161**, 43.
21 M. J. Adams and G. F. Kirkbright, *Analyst*, 1977, **102**, 281.
22 R. T. Swimm, *Appl. Phys. Lett.*, 1983, **42**, 955.
23 O. Pessoa, C. L. Cesar, N. A. Patel, H. Vargas, C. C. Ghizoni and L. C. M. Miranda, *J. Appl. Phys.*, 1986, **59**, 1316.
24 A. Rosencwaig and A. Gersho, *J. Appl. Phys.*, 1976, **47**, 64.
25 H. S. Carslaw and J. C. Jaeger, in *Conduction of Heat in Solids*, Clarendon, Oxford, 1973.
26 V. N. Bogomlov, M. S. Ivanova, V. P. Petranovskii, V. V. Pobor-chii, V. G. Slov'ev and S. I. Shagin, *Sov. Tech. Phys. Lett.*, 1991, **17**, 403.
27 A. Mandelis, in *Photoacoustic and Thermal Wave Phenomena in Semiconductors*, North Holland, New York 1987, p. 360.
28 J. Caetano de Souza, A. Ferreira da Silva and H. Vargas, *J. Phys. IV*, 1994, **4**, C7.
29 Z. K. Tang, Y. Nozue and T. Goto, *J. Phys. Soc. Jpn*, 1991, **60**, 2090.
30 R. Zallen, *The Physics of Amorphous Solids*, Wiley, New York, 1983, p. 20.

Paper 5/07953E; *Received 6th December*, 1995